Lehigh University
Lehigh Preserve

Theses and Dissertations

1988

An upper-bound approach to liquid lubricated friction during steady state sliding /

Tao Liu
Lehigh University

Follow this and additional works at: https://preserve.lehigh.edu/etd

Recommended Citation
Liu, Tao, "An upper-bound approach to liquid lubricated friction during steady state sliding /" (1988). *Theses and Dissertations*. 4842.
https://preserve.lehigh.edu/etd/4842

This Thesis is brought to you for free and open access by Lehigh Preserve. It has been accepted for inclusion in Theses and Dissertations by an authorized administrator of Lehigh Preserve. For more information, please contact preserve@lehigh.edu.

An Upper-Bound Approach To Liquid Lubricated Friction During Steady State Sliding

by

Tao Liu

A Thesis

Presented to the Graduate Committee

of Lehigh University

in Candidacy for the Degree of

Master of Science

in

Department of Materials Science
and Engineering

Lehigh University

December 10, 1987

Certification of approval

This thesis is accepted and approved in the partial fulfillment of the requirments for the degree of master science.

Date Nov 18 1987

Professor in charge

Chairman of department

Table of Contents

1 Abstract 0
2 Nomenclature 1
3 Introduction 3
  3.1 The role of asperities 3
  3.2 Subsurface plastic flow 6
4 Incorperation of Lubrication into the Model 9
  4.1 Description of the Model 9
  4.2 Mathematical treatment 11
5 Derivation of the Governing Equation 14
  5.1 Eddy Flow of Trapped Lubricant 14
  5.2 Hydrodynamic Lubrication 18
6 Discussion 19
  6.1 Global friction coefficient versus Sommerfeld number 21
  6.2 The extension of the surface deformation 23
  6.3 Effect of applied force on lubrication 24
  6.4 The transition region from mixed lubrication to hydrodynamic lubrication 25
7 Conclusion 26
8 Acknowledgement 27
9 Appendix A 28
10 References 29
11 Figures 31
  11.1 Fig.<1> The mobility of the ridge 31
  11.2 Fig.<2> Several patterns of distortion 32
  11.3 Fig.<3> Tri-triangular velocity field. 33
  11.4 Fig.<4> Schematic description of the growth of the ridge with increasing force 34
  11.5 Fig.<5> Schematic showing of flow pattern of the trapped fluid 35
  11.6 Fig.<6> Velocity field of trapped fluid 36
  11.7 Fig.<7> Global friction coefficient vs. Sommerfeld number, at constant pressure. m_0 is the local friction factor 37
  11.8 Fig.<8> The extension of the plastically deformed region vs. Sommerfled number, at constant pressure 38
  11.9 Fig.<9> The height of asperities vs. Sommerfeld number, at constant pressure 39
  11.10 Fig.<10> Global friction factor vs. applied force 40
12 Vita 41

1 Abstract

Presented in this paper is a study of the mathematical modeling of the steady state sliding of two metal surfaces, based on the upper bound approach, and including both the simulation of friction and of lubrication effects. The existence of wedge-shaped protrusions on the tool surface is assumed. Pressing these protrusions into the workpiece and sliding the tool along the workpiece produces asperities on its surface. Therefore, the formation of these asperities is caused by the plastic deformation through a specified depth under the surface. Growth of these asperities is arrested by the high pressure developed in the thin layer of lubricant trapped in the gaps between the asperities of the interfacing surfaces. The combination of the energy dissipated in the deformation of a thin layer under the surface, local resistant force to sliding along the interface, and the energy consumed in the lubricant produces a global resistance to sliding. The global resistance to sliding is a function of a Sommerfeld number, which is a dimensionless parameter : $S=\frac{\eta \cdot U}{\sigma_0 \cdot l}$, where η is the viscosity, U is the working speed, σ_0 is the flow strength of the workpiece, and l is average length of wedges. Global resistance to sliding decreases with increasing values of S until the global resistance reaches a minimum value; it then increases with further increase in S. The minimum value of global resistance is reached when full seperation by a thin lubricant film is established between the two solids. This phenomenon is called " hydrodynamic lubrication ". The resistance to sliding is related to the geometry of the asperities at the surface of the tool, to the Sommerfeld number ,S, and also to the constant friction factor, which is used for measuring a local frictional force where metal-to-metal contact prevails along the interfaces of the opposing asperities.

2 Nomenclature

a : distance from the origin to the point of intersection of the moving plate with the stationary plate

$\boldsymbol{F}_{tot}$: global resistance force

$\boldsymbol{F}_{hydro}$: frictional resistance during the stage of hydrodynamic lubrication

h : maximum of h_1

h_1 : ridge height

h_2 : extent of plastic deformation below the ridge

H : h_1 plus h_2

J_{tot} : totally consumed energy

l : total length of a wedge, also the length of stationary plate

l_0 : length of a ridge

l_1 : distance from projecting point of $\boldsymbol{C}$ onto horizontal plane to $\boldsymbol{D}$

l_2 : distance from projecting point of $\boldsymbol{C}$ onto horizontal plane to $\boldsymbol{B}$

m_0 : local constant friction coefficient

$\boldsymbol{N}$: normal force on the interface of wedge and ridge

$\boldsymbol{P}_{tot}$: applied total force

P_{hydro} : pressure in fluid during the stage of hydrodynamic lubrication

P_1 : pressure in fluid during the stage of boundary lubrication

r : radial coordinate

S : Sommerfeld number, $S=\frac{\eta \cdot U}{\sigma_0 l}$

$\boldsymbol{T}$: tangential force on the interface of wedge and ridge

$\boldsymbol{T}_1$: shearing force in viscous fluid

U : processing speed of a certain metal forming process

V : speed of Γ_7

x : coordinate of a point in fluid region

α : inclined angle between moving plate and stationary plate

α_1 : wedge angle

β_1 : wedge angle which is opposite to angle α_1

β_2 : angle between Γ_5 and horizontal line

Γ_i : boundaries of triangles, i = 1, 2, ... 8

θ : polar coordinate

θ_1 : polar coordinate of zero velocity point

θ_2 : polar coordinate of point at which velocity field changes direction

η : dynamic viscosity

σ_0 : yield strength of softer material

τ : shear stress of viscous fluid

3 Introduction

3.1 The role of asperities

Resistance exists to the relative interfacial movement of any two solid surfaces in contact. Since the time of Amontons (1699) (Ref. [1]), a great number of theories on the nature of friction have been developed. Coulomb (Ref.[2]) established the basic law of friction, and although he recognized that adhesion might play some part in friction, he considered that the major factor involved the interaction of surface roughness. He suggested that sliding involved the riding of rigid asperities on one surface over the other. Consequently, he produced the formula which states that the coefficient of friction is equal to tangent of the average asperity angle, and is independent of the load or the area of the interface. However, Leslie (Ref.[3]) pointed out that the simple roughness model of Coulomb is a non-dissipative process which occurs near the interface and which causes the onset of severe subsurface deformation.

More modern understanding has recognized that there are three major elements which play important roles in the friction of unlubricated solids (Ref.[4]):

1. The area of true contact between the sliding surfaces
2. The type and strength of bond that is formed at the contact interface
3. The way in which the material in and around the contacting regions is sheared and ruptured during sliding

There are many theories exploring the nature of surface deformation. One specific study by Wanheim (Ref.[5]) assumed that the flat surface was covered with a host of asperities. These asperities undergo plastic deformation as the

two surfaces slide relative to each other. As the harder tool advanced, the ridge underneath penetrated down into the softer workpiece, while a bulge of deformed material formed ahead of the tool. Using a slip line field, the power of deformation was calculated. Therefore, through the process of optimization, the shear stress and friction were estimated together with the depth of the surface layer.

Wanheim and Abildgaard (Ref.[6]) performed experiments to simulate the mobility of the asperities. In their experiments, Fig.<1>, a cylindrical rod, on which a ridge was initially machined circumferentially, was pushed through the die, the ridge stayed with the die, moving from the top end of the rod to the bottom. In order to observe subsurface events, the original rod was made of two sections joined together and held concentrically by a pin. The joined interface was originally a flat surface perpendicular to the axis of symmetry. After the die and ridge passed over the joined interface, the part of the flat surface that was near the outer cylindrical surface was dragged in the direction of motion of the die and ridge. The shape of the interface revealed the depth to which the skin of the rod had plastically deformed during the movement of the ridge. On the basis of the ridge experiment, Wanheim and Abildgaard proposed a slip line field which provided a plastic deformation mode for the ridge and a thin layer beneath it and which accommodated the transfer of a ridge. Wanheim and Abildgaard's slip line field provides for the suppression of the ridge immediately under the die, causing the ridge to penetrate the subsurface of the workpiece, and resulting in the rise of a wedge of deformed material in front of the tool. The ridge moves up and down and minutely forward, like an ocean wave. While the shape of the ridge is mobile, the material points remain

nominally in their original vicinity.

Further evidence for the mobility of the deformed asperities during the course of sliding of two contacting surfaces with different lubricant conditions and different wedge angles was obtained by Challen, et al (Ref.[7]). In his experiments, a hard wedge was vertically indented into the horizontal surface of a relatively soft aluminium-magnesium alloy specimen. Subsequently, the specimen was moved relative to the wedge in a direction normal to the edge of the wedge, and parallel to its surface. The test specimens were made in pairs of the same size, so that deformation could be measured on the center plane of the specimens. In order to vary the interfacial film strength, the tests were conducted under different lubricant conditions: (1) a boundary lubricant, (2) a straight mineral oil and (3) no lubrication. To observe the effects of wedge angle on ridges, these investigators varied the nominal wedge angles, ranging from 5 degrees to 45 degrees in steps of 5 degrees.

Their results showed that when a test specimen moved horizontally after initial indentation, the wedge first penetrated deeper as the vertical force was transferred to a single face of the wedge. It then reemerged while material deformed plastically by this face. Depending upon the conditions (wedge angle and lubrication), either a steady state with a plastic wave pushing along the original surface, (as shown in Fig.<5> of Ref.[7]), or a non-steady state with cracks occurring in the deformed material, (as shown in Fig.<7> of Ref.[7]), results. Challen, et al (Ref.[7]) also derived an analytical solution using the slip line technique to determine friction.

3.2 Subsurface plastic flow

Using a method similar to Wanheim's, Avitzur and coworkers(Refs. [8]-[10]) approached the friction behavior between two interfaces through a model involving the interaction of a rigid asperity and a deformable asperity. The asperities on surfaces are assumed to be triangular-shaped. While two surfaces are in contact and sliding relative to each other, wedges on one surface interact with ridges on the other. The deformation of the asperities may vary with their characteristics. Under different conditions, we may expect different flow patterns for the asperities. Fig.<2>, shows some different types of motion and deformation of the asperities. In Fig.<2a> the asperity is mobile. In Fig.<2b> the asperity shears off. In Fig.<2c> the surface is plowed. In Fig.<2d> the asperity is shaved. This displacement is possible because of plastic deformation that occurs in a thin layer underneath the surface of the softer solid.

From the studies of Avitzur and coworkers (Ref.[8],[9]), we know that the movement of the asperities leads to plastic deformation of a thin layer . This is the major part of the energy consumption which relates to the global frictional resistance. To describe the movement and plastic deformation of asperities, Avitzur (Ref.[9]) introduced the tri-triangular velocity field. This method is used to study the development of a of the model of steady state flow. With his method, the ridge and the region of plastic deformation underneath the surface are described through the movement of triangles I, II, and III (Fig.<3>). (Note : The significance of Zone IV will be described in Section 5.1) The energy consumed can be calculated through the energy dissipated by the three moving triangular sections. This calculation is achieved

by an upper-bound approach as follows:

An admissible velocity field composed of three triangles was proposed for the deformation zone and the upper-bound method was used in order to determine the power dissipation of the process. In Fig.<3>, a two-dimensional plane strain picture of a model is used to represent an asperity. The deformation region is divided into three rigid bodies designated by zones I, II, and III. The model has seven boundaries: Γ_1, Γ_2, Γ_3, Γ_4, Γ_5, Γ_6 and Γ_7. The surface Γ_1 is the interface between the tool and the ridge. Sliding occurs along the surface as the material moves forward at a velocity U. Shearing occurs over the surfaces of velocity discontinuities Γ_3 and Γ_4. Γ_7 is a free surface. The plastic deformation region near the surface of the workpiece was described through the motion of three triangular regions, each acting as a rigid body with linear motion. The stationary tool of Fig.<3> blocked the way for the ridge to move horizontally with the bulk of the workpiece. Thus, triangle ***DCE*** slid in the direction shown in Fig.<3>, parallel to the surface Γ_7 of the ridge of the workpiece. Triangle ***ECF*** moved in the horizontal direction, and triangle ***FCB*** penetrated into the workpiece. Because of the volume constancy requirement, a volume of material had to escape from the workpiece at an identical rate to that penetrating in the workpiece.

The flow of the triangles of Fig.<3> is similar to the flow through inclined converging planes whose upper bound solution has already been derived in Ref.[11] using a uni-triangular field. The individual triangles I and III can both be treated directly by the model of flow through inclined converging planes because of the similarities of their velocity fields. By also taking into account the shear loss along the additional surface Γ_6; the energy consumed in the

plastic deformation region can be calculated. (*see* Ref.[8])

When an asperity on the surface of a tool is pressed onto the surface of a workpiece, it indents the workpiece minutely and produces a ridge in the workpiece. The higher the pressure, the larger the ridge will be. At each given pressure, the ridge assumes an optimum shape and moves steadily as the workpiece slides relative to the tool. In the previous papers by Avitzur and coworkers, the resistance to sliding of unlubricated surfaces was studied. In this present thesis, the contribution from the trapped lubricants to the global frictional resistance is added.

4 Incorperation of Lubrication into the Model

4.1 Description of the Model

In the paper by Avitzur and Nakamura (Ref.[10]), ridge growth Fig.<4> was divided into two stages, the first stage being defined as the period prior to the ridge reaching the top of the wedge. During this stage, the size of the ridge increases with an increase in pressure. In the study of friction of unlubricated solids, the ridge height reaches the top of a wedge and then fills up the wedge. However, when lubricants exist as modeled in the present work, the ridge growth cannot reach the top of the wedge. When a lubricant fills gaps at the interface between a ridge and wedge, some of the normal load between the surfaces is transmitted through the trapped lubricant. As the speed increases, more load is carried through higher liquid pressure; therefore, a smaller ridge is produced on the softer surface. Thus, the lubricant moves along with the mobile ridge. Relative motion between the trapped fluid and the tool occurs as the fixed position of the tool is set. Consequently, the trapped lubricant moving at a relatively high speed produces a rather high pressure, exerted on the interfaces of tool and workpiece. This pressure will arrest the growth of the ridge, or even stop the growth. To minimize the energy consumed, the ridge will adjust its shape to be some optimal profile, causing the geometric parameters of the ridge to change.

As previously discussed, fluid can be trapped in the gap between a wedge and a ridge, causing the cavity to be filled by the trapped lubricant. In Fig.<3> the clearance region is designated as zone IV. For the sake of simplification of the mathematical treatment, it is assumed that the characteristic length of Γ_7 is greater than the clearance thickness. Based on

this assumption, we may assume surface Γ_7 to be infinite in its extent. Moreover, both Γ_7 and Γ_8 are assumed to have infinite width so that the flow may be considered two-dimensional. Therefore, no component of velocity appears in the direction perpendicular to the plane of the paper, as is shown in Fig.<5>. Even though high velocities may be involved, the thickness of the lubricant film is so small that the Reynolds number is far below its critical value for this system. Thus, inertial effects may be neglected, and laminar flow is assumed. Thermal effects cannot always be neglected, but we can still assume a constant viscosity, and constant density. With the preceding hypothesis, we are studying two-dimensional Stokesian flow.

The primary function of the lubricant is to separate the bearing surfaces. As long as the lubricant is effective, there is no metal-to-metal contact between bearing surfaces. If the lubricant film keeps the interfaces apart when they are in relative motion, then it must be capable of sustaining a load, particularly, the very high pressure in the metal working processes. Under these circumstances, the pressure in the lubricant must increase from the pressure Po at one end of the passage in Fig.<6>, pass through a maximum value, and return to Po at the other end of the passage. This is possible only if the passage varies with x in a certain proper way. Fig. <6> shows the simplest way in which the passage should be varying with x. The two surfaces in Fig.<6> are planes and inclined to one another in the direction of motion. The angle between the two inclined surfaces is α (In practice this angle is very small and it is greatly exaggerated in Fig. <6>).

The model we will deal with is the limiting case of general flow described in the preceeding paragraph. In other words, what one is most concerned with

here is the case that when point A on plane Γ_8 in Fig.<6a> approaches to plane Γ_7. In this limiting case, the center of pressure in the lubricant is approaching the intersection point O, and the pressure at this point is reaching infinity. This limiting situation cannot occur in practice, but for analysis, we will keep the distance between point A and plane Γ_7 as small as possible to attain the best approximation to our modeling.

In Fig.<3> it can be seen that the boundary $OADC$ is so complicated that it is very difficult to propose a proper boundary condition to it. To circumvent the difficulties, we need an approximation to the boundary condition on Γ_5, Γ_7, and the pressure distribution in the fluid. Based on this consideration, we take the model shown in Fig.<5> and Fig.<6> to approximate our case. Here, the boundary effect of both ends of the narrow passage on the flow of lubricant is neglected. Also, in this particular occurance, we may expect that the pressure reaches its maximum value at the upper end of the narrow passage, neglecting the pressure boundary condition at the other end.

4.2 Mathematical treatment

Consider the force balance on the ridge, which is governed by the equation below :

$$\begin{aligned} \boldsymbol{P}_{tot} &= \boldsymbol{N}\cos\alpha_1 - \boldsymbol{T}\sin\alpha_1 + \boldsymbol{P}_l\cos\alpha_1 - \boldsymbol{T}_l\sin\alpha_1 \\ \boldsymbol{F}_{tot} &= \boldsymbol{N}\sin\alpha_1 + \boldsymbol{T}\cos\alpha_1 - \boldsymbol{P}_l\sin\alpha_1 + \boldsymbol{T}_l\cos\alpha_1 \end{aligned} \qquad (5.1)$$

where $\boldsymbol{N}$ and $\boldsymbol{T}$ are the normal and the tangential force on the surface Γ_1, respectively (*see* Fig.<2> in Ref.[10]). Here we only give the expression for $\boldsymbol{T}$ as

$$\boldsymbol{T} = \frac{\sigma_0}{\sqrt{3}} \frac{m_0 \cdot h_1}{\sin\alpha_1} \qquad (5.2)$$

The terms $\boldsymbol{P}_l$ and $\boldsymbol{T}_l$ in Eq.(5.1) are the pressure exerted by the trapped

fluid on the ridge and the shear stress in the trapped lubricant, respectively, and they are given below (*see* the derivation of these terms in **section 6**):

$$\boldsymbol{P}_l = \eta U g(\beta_1,\beta_2)[\ln\frac{r_2}{r_1} - (1-\frac{r_1}{r_2})] \tag{5.3}$$

$$\boldsymbol{T}_l = \frac{\eta U}{\alpha}\ \ln\frac{r_2}{r_1}\ g(\beta_1,\beta_2) \tag{5.4}$$

where $g(\beta_1,\beta_2)$ is given in Eq.(5.7). After eliminating $\boldsymbol{N}$ from the Eqn.(5.1), we express the relation between $\boldsymbol{P}_{tot}$, the total pressure, and $\boldsymbol{F}_{tot}$, the total resistance to sliding:

$$\frac{\boldsymbol{P}_{tot}}{\sigma_0 l} = \frac{\boldsymbol{F}_{tol}}{\sigma_0 l}\cot\alpha_1 - \frac{m_0}{\sqrt{3}}\frac{h_1}{l}\frac{1}{\sin^2\alpha_1} + \frac{S}{\sin\alpha_1}\{[\ln\frac{r_2}{r_1} - (1-\frac{r_1}{r_2})]\sin 2\alpha_1 + \frac{1}{\alpha}\ln\frac{r_2}{r_1}\}g(\beta_1,\beta_2) \tag{5.5}$$

In order to determine the geometrical parameters appearing in the above relation of Eqn.(5.5), the total energy dissipated in the deformation area (including the fluid region) is taken into account, and we obtain the following relation:

$$\begin{aligned}\frac{\boldsymbol{J}_{tot}}{\sigma_0 U l} &= \frac{1}{\sqrt{3}}\frac{1}{h_2\cot\beta_1 + x_2}\{x_2^2 + h_2^2 + \frac{h_2}{H}[(l_2 - x_2)^2 + H^2]\} \\ &+ \frac{1}{\sqrt{3}}\frac{1}{h_2\cot\alpha_1 + x_1}\{x_1^2 + h_2^2 + \frac{h_2}{H}[(l_1 - x_1)^2 + H^2] + m_0 h_1 h_2\frac{1}{\sin^2\alpha_1}\} \\ &+ \frac{1}{\sqrt{3}}(1-\frac{h_2}{H})(l_0 - x_1 - x_2) + \frac{S}{\alpha}\ln\frac{r_2}{r_1}[g(\beta_1,\beta_2)]^2\end{aligned} \tag{5.6}$$

By optimization of $\boldsymbol{J}_{tot}$ with respect to the geometrical parameters, we can determine the optimal values of these geometrical parameters; the optimal geometrical values minimize the relative power. All the parameters are listed below:

$$h = \frac{1}{2}\tan\alpha_1$$

$$\frac{r_2}{r_1} = \frac{1 - \frac{l_0}{l}}{1 - \frac{h_1}{h}}$$

$$\alpha = \beta_1 - \alpha_1$$

$$\beta_1 = \tan^{-1}\left[\frac{1}{\frac{l_0}{h_1} - \cot\alpha_1}\right]$$

$$\beta_2 = \tan^{-1}\frac{h_2}{x_2}$$

$$g(\beta_1,\beta_2) = \frac{\sin\beta_2}{\sin(\beta_1 + \beta_2)} \qquad (5.7)$$

When hydrodynamic lubrication commences, the friction resistance is given as

$$\frac{F_{hydro}}{\sigma_0 l} = \frac{1}{2}\frac{P_{hydro}}{\sigma_0 l}\tan\alpha_1 + \frac{S}{\tan\alpha_1}\ln\frac{a}{a-l} \qquad (5.8) \qquad (\text{see Eq.(6.19)})$$

and the pressure takes the following form

$$\frac{P_{hydro}}{\sigma_0 l} = \frac{6S}{\tan^2\alpha_1}\left(\ln\frac{a}{a-l} - \frac{2l}{2a-l}\right) \qquad (5.9) \qquad (\text{see Eq.(6.20)})$$

These two sets of equations describe the behavior shown in Fig.<7>. Eq.(5.6) describes the characteristic behavior of the boundary lubrication before the hydrodynamic commences; during this period, the global frictional resistance is due to both sublayer plastic deformation induced by the indentation and the energy dissipated in the trapped lubricant. As the pressure remains constant during the process, Eq.(5.6) indicates a monotonic decrease in the global friction, and the pressure produced by the lubricant increases as the Sommerfled number increases. At a certain critical point, where the indentation diminishes, the hydrodynamic lubrication begins; Eq.(5.7) is used to illustrate this condition. Consequently, there is a drastic drop in the global frictional resistance once the hydrodynamic lubrication begins.

5 Derivation of the Governing Equation

5.1 Eddy Flow of Trapped Lubricant

The flow pattern of the trapped fluid is shown in Fig. <5>. In order to describe this behavior quantitatively, we must first establish a coordinate system. The origin of the coordinates is chosen so that the intersection point of planes Γ_8 and Γ_7, or their extention, is at $r = 0$. The workpiece in Fig. <2> moves relative to the tool with constant velocity U. Therefore, plane Γ_7 moves relative to plane Γ_8 with velocity V in the r direction. The angle between these two planes is α. A position of a point in the lubrication region is measured by its radial coordinate r and its angle θ.

The prevailing concept today is that when viscous fluid is in contact with the surface of a solid, the fluid at that interface is moving in unison with the solid. Thus, the velocity of the lubricant must equal the relative velocity V of the plane Γ_7 when θ is zero, and also be equal to zero when $\theta = \alpha$. From the principles of continuity and imcompressibility, the volume of lubricant flowing through each cross section is constant, and for trapped lubricant, this constant is zero. Simple arithmetic and application of the concept of minimum energy to shear power losses in a viscous matter (liquid) result in the finding that the velocity field has a piecewise linear distribution with respect to the angle θ. For visualization this distribution is schematically shown in Fig. <6a>. Furthermore, the component of velocity in the θ direction is neglected because the lubricant layer is very thin. According to the previous considerations, we deduce the velocity field as follows:

Assume

$$v_r = \begin{cases} \dfrac{C_1}{r}(\theta-\alpha), & if \quad 0 \le \theta \le \theta_2 \\ \dfrac{C_2}{r}+V, & if \quad \theta_2 \le \theta \le \alpha \end{cases} \tag{6.1}$$

where

$$V = Ug(\beta_1,\beta_2),$$

and

$$g(\beta_1,\beta_2) = \frac{\sin\beta_2}{\sin(\beta_1+\beta_2)} \tag{6.2}$$

The constants, C_1, C_2 and θ_2 are determined below. The volume of lubricant passing through section I in Fig.<6a> is

$$V_1 = \int_0^{\theta_1} v_r r\, d\theta = \frac{C_1}{2}\theta_1^2 + Vr\theta \tag{6.3}$$

where V is the velocity of lubricant on Γ_7, which will be given as a boundary condition below. The volume of lubricant passing through section II in Fig. <6a> is

$$V_2 = \int_{\theta_1}^{\alpha} v_r r d\theta = \frac{C_1}{2}(\theta_2-\theta_1)^2 + V\cdot r(\theta_2-\theta_1) - \frac{C_2}{2}(\alpha-\theta_2)^2 \tag{6.4}$$

These two volumes are equal because the total liquid passing through any cross section of the trapped lubricant is zero.

$$V_1 = V_2 \tag{6.5}$$

On the other hand, because of the continuity of the velocity distribution at $\theta = \theta_2$, it can be demonstrated that

$$\frac{C_1\theta_2}{r} + V = \frac{C_2}{r}(\theta_2-\alpha)$$

or upon rearrangement that

$$C_1\theta_2 + rV = C_2(\theta_2-\alpha) \tag{6.6}$$

Setting

$$\theta_2 = \frac{\theta_1 + \alpha}{2}$$

$$C_2 = -C_1$$

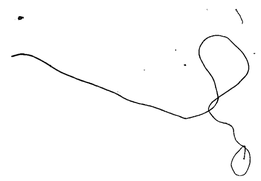

we obtain from Eqn.(6.6)

$$C_1 = -\frac{rV}{\theta_1}$$

Inserting C_1 back into Eqn. (6.5) we obtain

$$\theta_1 = \frac{\alpha}{2}$$

Substituting all these parameters into the expression of the velocity field Eqn. (6.1), we finally attain the velocity distribution in the r direction

$$v_r = \begin{cases} -\frac{2V}{\alpha}(\theta - \frac{\alpha}{2}), & 0 \leq \theta \leq \frac{3\alpha}{4} \qquad (6.7a) \\ \frac{2V}{\alpha}(\theta - \alpha), & \frac{3\alpha}{4} \leq \theta \leq \alpha \qquad (6.7b) \end{cases}$$

v_r is a piecewise continuous function. The change in sign between Eq.(6.7a) and Eq.(6.7b) represents two different directions of the flow on the two cross sections.

Substituting the velocity from Eqn.(6.7) into the Navier-Stokes momentum equation, the momentum equation for negligible fluid film thickness is approximated (for the assumption that pressure is independent of θ) through the following differential equation for the pressure distribution in the trapped lubricant:

$$\frac{dp}{dr} = \eta(\Delta v_r - \frac{v_r}{r^2}) \qquad (6.8)$$

where

$$\Delta v_r = \frac{1}{r}\frac{\partial}{\partial r}(r\frac{\partial v_r}{\partial r}) + \frac{1}{r^2}\frac{\partial^2 v_r}{\partial \theta^2} + \frac{\partial^2 v_r}{\partial \theta^2} \qquad (6.9)$$

By integration of Eqn.(6.7) with respect to r, the pressure distribution is

found to be

$$p=\eta v_r \frac{r_2 - r}{r r_2} \tag{6.10}$$

Integrating Eqn.(6.10) with respect to r, and setting θ equal to 0, we obtain the total normal force exerted by the trapped lubricant on the ridge as :

$$p_l=\eta U g(\beta_1,\beta_2)[\ln \frac{r_2}{r_1} - (1 - \frac{r_1}{r_2})] \tag{6.11}$$

The energy density (energy per unit volume) consumed in the fluid is

$$j_l=\frac{1}{4}\eta \epsilon_{r\theta}^2 \tag{6.12}$$

and the shear strain rate is

$$\epsilon_{r\theta} = \frac{1}{r}\frac{\partial u_r}{\partial \theta} + \frac{\partial u_\theta}{\partial r} - \frac{u_\theta}{r} \tag{6.13}$$

With the preceding velocity field (Eq.(6.7)) we obtain the shear strain rate as follows:

$$\epsilon_{r\theta} = \begin{cases} -\frac{2V}{r\alpha}, & 0 \le \theta \le \frac{3\alpha}{4} \\ \frac{2V}{r\alpha}, & \frac{3\alpha}{4} \le \theta \le \alpha \end{cases} \tag{6.14}$$

Substituting the shear strain rate from Eqn.(6.14) into Eqn.(6.12), and integrating Eqn.(6.12) through the domain of the lubricant, the total energy dissipated in the fluid is:

$$J_l=\frac{\eta U^2}{\alpha}\ln \frac{r_2}{r_1} [g(\beta_1,\beta_2)]^2 \tag{6.15}$$

To express the results in a dimensionless form, we divide Eqn.(6.11) and Eqn.(6.15) by the yield strength of workpiece and the characteristic length of a ridge, and obtain the dimensionless pressure distribution of the fluid as follows,

$$\frac{p_l}{\sigma_0 l}=S\cdot g(\beta_1,\beta_2)[\ln \frac{r_2}{r_1} - (1 - \frac{r_1}{r_2})] \tag{6.16}$$

The power is given by

$$\frac{J_l}{\sigma_0 U l} = \frac{S}{\alpha} \ln \frac{r_2}{r_1} |g(\beta_1,\beta_2)|^2 \qquad (6.17)$$

5.2 Hydrodynamic Lubrication

The above model prevails only for boundary lubrication. When hydrodynamic lubrication prevails, the conventional equations for this later mode are adopted (Ref. [12] and [13]). These equations are given below:

The pressure in the lubricant is given as

$$p_{hydro} = p_0 + \frac{6\eta U x(l-x)}{\tan^2 \alpha_1 (a-x)^2 (2a-l)} \qquad (6.18)$$

The load which such a system can support is determined by the total net thrust which the fluid exerts on a unit width of either bearing surface. This is given by

$$P_{hydro} = \frac{6 \cdot \eta \cdot U}{\tan^2 \alpha_1} \left(\ln \frac{a_p}{a-l} - \frac{2l}{2a-l}\right) \qquad (6.19) \qquad \text{(see Eqn. (5.8))}$$

The total force resisting the movement of the sliding surfaces is

$$F_{hydro} = \frac{P_{hydro} \tan \alpha_1}{2} + \frac{\eta \cdot U}{\tan \alpha_1} \ln \frac{a}{a-l} \qquad (6.20) \qquad \text{(see Eqn. (5.9))}$$

At this point, several questions arise:

1. When does the hydrodynamic lubrication start to prevail?
2. How do we determine the start of hydrodynamic lubrication?

Section 7 will explore and discuss these two aspects.

6 Discussion

In the previous section, we have derived an upper-bound model for the energy consumption in trapped lubricant. We have also described the deformation of the sublayer to occur as a result of the plastic deformation energy of the nominal surface layer. We will now use this upper-bound solution to relate the frictional resistance to the externally applied force, to the speed of metal forming processes, and to the extension of the plastically deformed sublayer.

As stated before, the total frictional resistance is the sum of the two power terms. One is the power consumed in the lubricant, the other is the power dissipated in the plastically deformed sublayer. We have already analyzed the linear distribution of the fluid velocity field which produces the minimun energy consumption required by the upper-bound approach. The extent of the deformed sublayer is governed by the principle of minimum energy, which states that any physical process takes the form that can optimize (minimize) the energy consumption for the process.

The necessary condition for the deformation energy to take the minimum value is that the partial differentials of the frictional power with respect to the psuedo-independent parameters must be zero. In the present modeling x_1, x_2, the coordinate points of the triangles in Fig.<3>, h_2, the depth of deformed sublayer, and l_0 , the length of a ridge, are all pseudo-independent parameters. They are pseudo-independent because the shape of the deformed asperities is determined by minimization of dissipated energy, and this shape is defined by these geometrical parameters. On the other hand, by optimizing the sum of the friction power dissipated by the lubricant and plastic deformation energy in the

softer material (Eq.(5.6)) with respect to the psuedo-independent parameters, the interaction between the nominal surface layer of the softer material and the lubricant can also be determined. Therefore, the effects of the existence of lubricants on the lubrication friction are explored and the characteristics of the lubrication friction can be determined.

Three significant relationships may be demonstrated as a result of the inspection of the solutions obtained:

1. The relation between global frictional factor and Sommerfeld number, while working at a constant external force;

2. The relation between the extension of the plastically deformed sublayer, which is indicated by the geometrical parameters of the tri-triangular velocity field, and the Sommerfeld number, also at constant external force;

3. The relation between the external force and the extension of the plastically deformed surface layer at constant Sommerfeld number;

For the following discussion, all the numerical data are given assuming the metal workpiece to be pure aluminium and the lubricant to be "master draw"[1]. Therefore, for a reasonable range in processing speed, U, the variation range for Sommerfeld number S, which is an input parameter in the calculation, is between 0.0 to 0.0015. In order to be coincident with Avitzur's previous work (Refs.[8],[9] and [10]), we set $\alpha_1 = 5^\circ$, $m_0 = 0.01$, and the applied force $\boldsymbol{P}_{tot}$ is taken in the range of $0.3\sigma_0$ to $1.1\sigma_0$ in Eq.(5.5) and Eq.(5.6).

[1]Lubricant used in wire drawing processes, manufactured by ETNA Product, Inc.

6.1 Global friction coefficient versus Sommerfeld number

Consider now, how the indentation model previously described is modified in the presence of a lubricant. Putting the above defined parameters into Eq.(5.5) and Eq.(5.6), and varying the Sommerfled number, S, from 0.0 to 0.0011 in steps of 0.0002, also varying the applied force, $\boldsymbol{P}_{tot}$, ranging from $0.3\sigma_0$ to $1.1\sigma_0$ in steps of $0.2\sigma_0$ and solving the two equations (*see the program Flow Pattern given in Appendix A*) for the pressure in the lubricant and for the global friction factor, $\frac{J_{tot}}{\sigma_0 Ul}$. The calculated lubricant pressure ranges from $0.0025\boldsymbol{P}_{tot}$ to $0.023\boldsymbol{P}_{tot}$ as S varies from 0.0 to 0.0011 (*see* Fig.<7a>). In Fig.<7b> and Fig.<7c> it shows the relationship between the global friction factor and the Sommerfeld number, the local friction factor m_0 and the wedge angle α_1 as parameters, respectively. It is therefore concluded that the effect of lubrication is such that the load is now distributed over an area including the lubricant film and minute metallic junctions formed through the lubricant film at the points where it is penetrated. In this calculation, the dynamic viscosity η remains constant. An increase in S is in fact just an increase in the sliding velocity, U. Therefore, it can be seen that the higher the sliding velocity, the more load can be distributed over the lubricant.

This calculation also indicates that at constant applied force $\boldsymbol{P}_{tot}$, the calculated global friction factor $\frac{J_{tot}}{\sigma_0 Ul}$ (*see Eq.(5.6)*) decreases monotonically with an increase in sliding velocity, U. For example, at an applied force $0.7\sigma_0$, the global friction factor decreases from 0.0619 to 0.057 as S increases from 0.0001 to 0.0011 (*see* Fig.<7a>). This tendency in the relation between the variation of global friction factor and sliding velocity may be physically explained as follows:

A lubricant used in a metal forming process adheres to the moving workpiece and enters the interface region between the die and the material. When the workpiece moves at very low speed, only one or a few atomic layers of lubricant will be interposed between the sliding surfaces. Therefore, a fluid film is formed at the interface and is able to reduce the amount of interaction between the two surfaces and is itself easily sheared. The thin film is penetrated by surface asperities; in regions adjacent to these asperities lubricant pools are formed which then spread over the interface. The liquid in these pools is trapped, and placed under pressure between the workpiece and the die. As the result of the penetration through the fluid film, the asperities on the harder surface may indent the softer material, resulting in the rise of a bulge in front of the advancing tool. According to the model of Wanheim and Abildgaard (Ref.[6]) , the ridge moves both up and down, similar to an ocean wave. Now what is happening to the liquid in the lubricant pools? Is the liquid just sitting there, being compressed by the working pressure? No. The liquid in the lubricant pools tries to find an escape route in order to set itself free and relieve the compressive load. Because of the viscosity of the lubricant, the lubricant layer immediately contacting the workpiece will move with the ridge at the same speed, while the opposite layer of the lubricant, at the die surface, does not move at all. A high velocity gradient is generated in the pool liquid. In the calculation given above, the maximum difference in the velocity on the two interfaces is 60 in./sec (as defined by the allowed variation in S). This gradient results in severe shear in the lubricant. The power generated by the resistance of the lubricant to shear, j_l, is proportional to the second power of the velocity gradient $\epsilon_{r\theta}$, as derived in **Section 6, Eq.(6.12)**. The pressure

in the pool liquid, P_l, also increases with increasing velocity, U. As the velocity increases, more and more lubricant is dragged into the sliding interface. Therefore, as the lubricant shear loss, $\boldsymbol{T}_l$U ($\boldsymbol{T}_l$ is given in Eq.(5.4)), contributes to a higher portion of the total frictional resistance, the pressure $\boldsymbol{P}_l$ in the fluid increases simultaneously in order to seperate the material and the die. At the same time, the pressure on the asperities decreases, and the indentation of the softer material also decreases. Therefore, the shear of metal in the nominal surface layer of the workpiece decreases, and the resultant friction $\boldsymbol{J}_{tot}$ is reduced. Finally, it is assumed at some higher speed, the two mating surfaces become fully separated by the lubricant. At this point, the hydrodynamic lubrication commences.

6.2 The extension of the surface deformation

It is found by solving Eq.(5.5) and Eq.(5.6) that h_2, the depth of plastic deformation, decreases with an increase in Sommerfeld number at constant applied force $\boldsymbol{P}_{tot}$. At the applied force of $0.7\sigma_0$, h_2 decreases from 0.126 to 0.092, as Sommerfeld number S increases from 0.0001 to 0.0011, i.e., a 28% reduction. The similar situation occurs in the other ranges of applied force, $0.3\sigma_0$, $0.5\sigma_0$, etc. The relation between h_2 and the Sommerfeld number S is shown in Fig.<8>. A direct conclusion can be drawn, which states that as the sliding surface is lubricated by fluid the extent of the plastic deformation of the subsurface, h_2, decreases as sliding velocity U increases.

Inspecting Eq. (5.3), it can be concluded that the lubricant in pools can support more load as the operating velocity increases. Consequently, asperity penetration through the liquid film decreases and the asperities on the softer material see a lower load , resulting in a decrease of both the ridge height, h_1,

and h_2 (Fig.<3>). It can be seen in Fig.<9>, that the height of a ridge h_1 decreases with an increase in Sommerfeld number S.

Making the above point is important, since these results show that the main function of a lubricant is to interpose a film between the sliding surfaces that is able to reduce the amount of solid interaction and consequently the extent of bulk plastic deformation in the nominal surface layer. While the operating velocity U is within the range of mixed lubrication, both friction resistance $\boldsymbol{J}_{tot}$ and wear, which is represented by h_1 (*see Ref.[9]*), can be greatly reduced, compared to the magnitudes during dry lubrication. Therefore, reduced indentation into the sliding surface can protect the surface from plowing and galling.

6.3 Effect of applied force on lubrication

The applied force has a remarkable effect on the lubrication processes. The previously described calculation (***Section 7.1***) also gives the following result: At constant Sommerfeld number S, the global friction factor increases as the applied force increases. For example, for S set at 0.0011, the global friction factor $\frac{\boldsymbol{J}_{tot}}{\sigma_0 Ul}$ increases from 0.025 to 0.087, as the applied load $\boldsymbol{P}_{tot}$ increases from $0.3\sigma_0$ to $1.1\sigma_0$. This is because a higher external load causes deeper penetration into the softer material. In the data offered here, the indentation, h_1, increases from 0.0082 for an applied force $0.3\sigma_0$, to 0.028 for an applied force $1.1\sigma_0$. The extent of the subsurface plastic deformation, h_2, increases from 0.043 at an applied force $0.3\sigma_0$, to 0.133 at an applied force $1.1\sigma_0$. An increase of 71% in h_1, and of 68% in h_2, are obtained respectively as the applied force is increased. This, of course, will greatly increase friction and wear. The curve of the applied force $\boldsymbol{P}_{tot}$ versus the global friction factor is shown in Fig.<10>.

In order to reach the hydrodynamic lubrication stage at higher applied load, the trapped lubricant must reach a higher velocity to establish enough pressure within the lubricant. Thus, hydrodynamic lubrication is established much later and with more difficulty at high applied load. This is why the Sommerfeld number of the intersection points of the hydrodynamic curves with those for mixed lubrication increases as the applied force increases (Fig.<7>).

6.4 The transition region from mixed lubrication to hydrodynamic lubrication

In the present model, we cannot quantitatively determine the transition point from mixed lubrication to hydrodynamic lubrication, i.e., quantitatively determine the intersection points in Fig.<7>. This is due to the precision of the modeling. We assumed that the flow of the trapped liquid is laminar. Therefore, we take the linear distribution of the velocity field of liquid as the upper-bound approximation to the real flow pattern, and we neglect the complexity of the surface geometry. In the real physical world, the assumption of laminar flow in the presence of high pressure may not be correct and a model which would use turbulent flow might be more realistic. If we could solve the difficult fluid mechanics problem, we may be able to quantify the transition region.

We can, however, make some prediction based on the present model. Our model shows an increasing tendency in pressure generated in the trapped liquid as the sliding speed increases. Thus, it may be deduced that the pressure in the liquid alone can exceed the applied loading as sliding speed reaches a critical value. At this point, the trapped lubricant begins to separate the two sliding surfaces fully, causing a drastic drop in the global frictional resistance.

7 Conclusion

In this thesis, discussion has focused on the effect of lubricant upon the sliding friction. The global friction factor is calculated for the case of mixed lubrication. For this stage of mixed lubricaton, the calculation of the friction factor has been quantified. We conclude that the friction is caused by the contributions of both internal shear of the lubricant film, and by the metal-to-metal contact of the high points on the workpiece and the die. With an increase in speed, (1) shear in the liquid rises moderately, while (2) fewer and fewer contacts are left between the workpiece and the die, which in turn lowers their contribution to friction. Based on the present modeling, the net effect of an increase in speed in the presence of a liquid lubricant, is a decrease in global friction as well as a moderate increase in liquid film thickness.

The following aspects should be considered in the future:

1. The viscosity of a lubricant is sensitive to a temperature change. A large amount of heat is generated in metal forming processes. Thus, in the future, the temperature effect should be included in the model.

2. From my experience, I think the assumption of a linear distribution of the velocity field gives too low a pressure in the liquid. This may be due to neglecting the angle effect upon trapped lubricant flow. The flow at the angle (Fig.<5>) may be treated as a vortex flow. Further we may be able to quantify the transition region from mixed lubrication to hydrodynamic lubrication.

3. Surface quality of the products produced during metal forming is another aspect of the lubrication problem. A surface failure model needs to be established which includes lubricant effects during forming processes.(*see* Ref.[14]).

8 Acknowledgement

I am grateful to Professor Avitzur for providing me with the opportunity to study in the United States. Under his guidance, and with financial support from the National Science Foundation grant, I was able to explore my field of study so that I may continue to acquire the skill and knowledge needed to perform further experimentation.

9 Appendix A

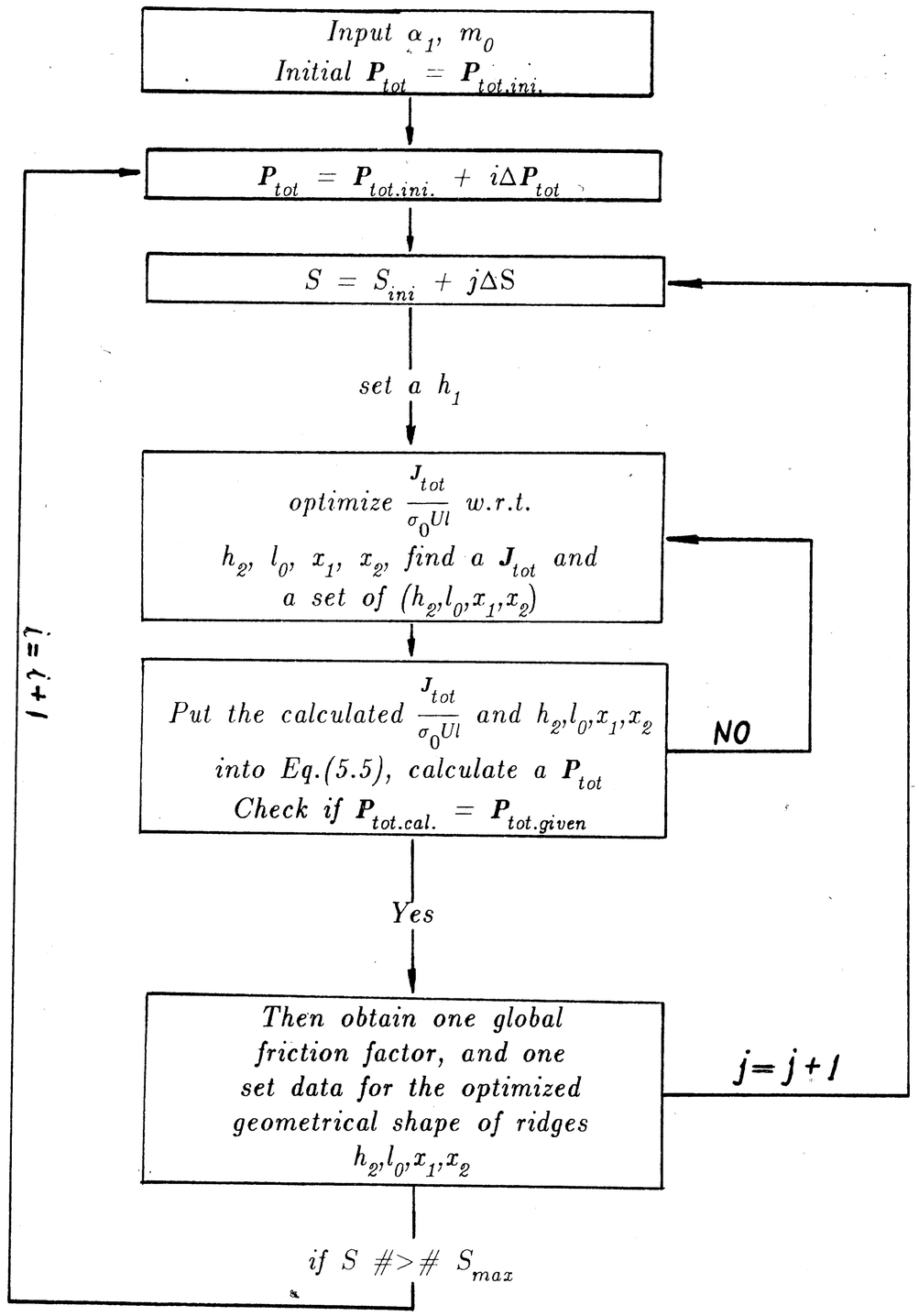
Input α_1, m_0
Initial $\boldsymbol{P}_{tot} = \boldsymbol{P}_{tot.ini.}$
$\boldsymbol{P}_{tot} = \boldsymbol{P}_{tot.ini.} + i\Delta\boldsymbol{P}_{tot}$
$S = S_{ini} + j\Delta S$
set a h_1
optimize $\frac{J_{tot}}{\sigma_0 Ul}$ w.r.t. h_2, l_0, x_1, x_2, find a $\boldsymbol{J}_{tot}$ and a set of (h_2,l_0,x_1,x_2)
Put the calculated $\frac{J_{tot}}{\sigma_0 Ul}$ and h_2,l_0,x_1,x_2 into Eq.(5.5), calculate a $\boldsymbol{P}_{tot}$
Check if $\boldsymbol{P}_{tot.cal.} = \boldsymbol{P}_{tot.given}$
NO
Yes
Then obtain one global friction factor, and one set data for the optimized geometrical shape of ridges h_2,l_0,x_1,x_2
j=j+1
if S #># S_{max}
i=i+1

10 References

1. Amontons, G., (1699), 'De la resistance caus'ee dans les machines', Memoires de l'Academie Royale, A, (Chez Gerard Kuyper, Amsterdam, 1706), 257-82.

2. Coulomb, C. A., (1785) 'Theorie des machines simples, en ayant egard au frottement de leurs partres, et a la roideur des cordages', Mem. Math. Phys., X, Paris, 161-342.

3. Leslie, John (1804)," An Experimental Inquiry into the Nature and Propogation of Heat", Printed for J. Newman, No.22. Poultry, also sold by Bell and Bradfute, Edinburg.

4. Tabor, D.," Friction - the present state of our understanding", J. Lubr. Tech., 103 (1981) 169-179.

5. Wanheim, T., and Abildgaard, T., " A mechanism for metallic friction". p.122 proc. 4th Int. Cof. on Production Eng., Tokyo, Aug. 1980.

6. Abildgaard, T., and Wanheim, T., " An investigation into the mechanisms of abrasive wear and processing of metals". pp.521-529 Proc. 2nd Cairo University Mechanical Design and Production Conf., Cairo, December 27-29, 1982, Cario University, Giza

7. Challen, J. M., Mclean, L. J., and Oxley, P. L. B., "Plastic deformation of a metal surface in sliding contact with a hard wedge : its relation to friction and wear". Proc. R. Soc. Lond. A394, 161-181 (1984)

8. Avitzur, B., Huang C. K. and Zhu, Y. D.," A friction model based on the upper-bound approach to the ridge and sublayer formations-update", pp.103-109 Proc. 13th North Am, Metalworking Reseach Conf. Berkley, CA, May 19-22, 1985, Society of Manufacturing Engineers, Dearbon, MI.

9. Avitzur, B., Huang, C. K., and Zhu, Y. D., "A friction model based on the upper bound approach to the ridge and sublayer deformations", Wear, 95, 59-77 (1984)

10. Avitzur, B. and Nakamura, Y., "Analytical determination of friction resistance as a function of normal load and geometry of surface irregularities", Wear, 107, 367-383 (1986).

11. Kiuchi, M., Avitzur, B., "Limit analysis of flow through inclined converging planes", J. Eng. Ind., ASME, 102, 109-116 (May 1980)

12. Wu, W. Y., Fluid mechanics (in Chinese), Chapter 7, pp. 207-213, University of Peking Press, Beijing, 1980.

13. Halling, J., Introduction to Tribology, London: Wykeham Publications, New York, Springer-Verlag, 1976

14. Suh, N., The delamination theory of wear, Wear, 25, 111-124 (1973)

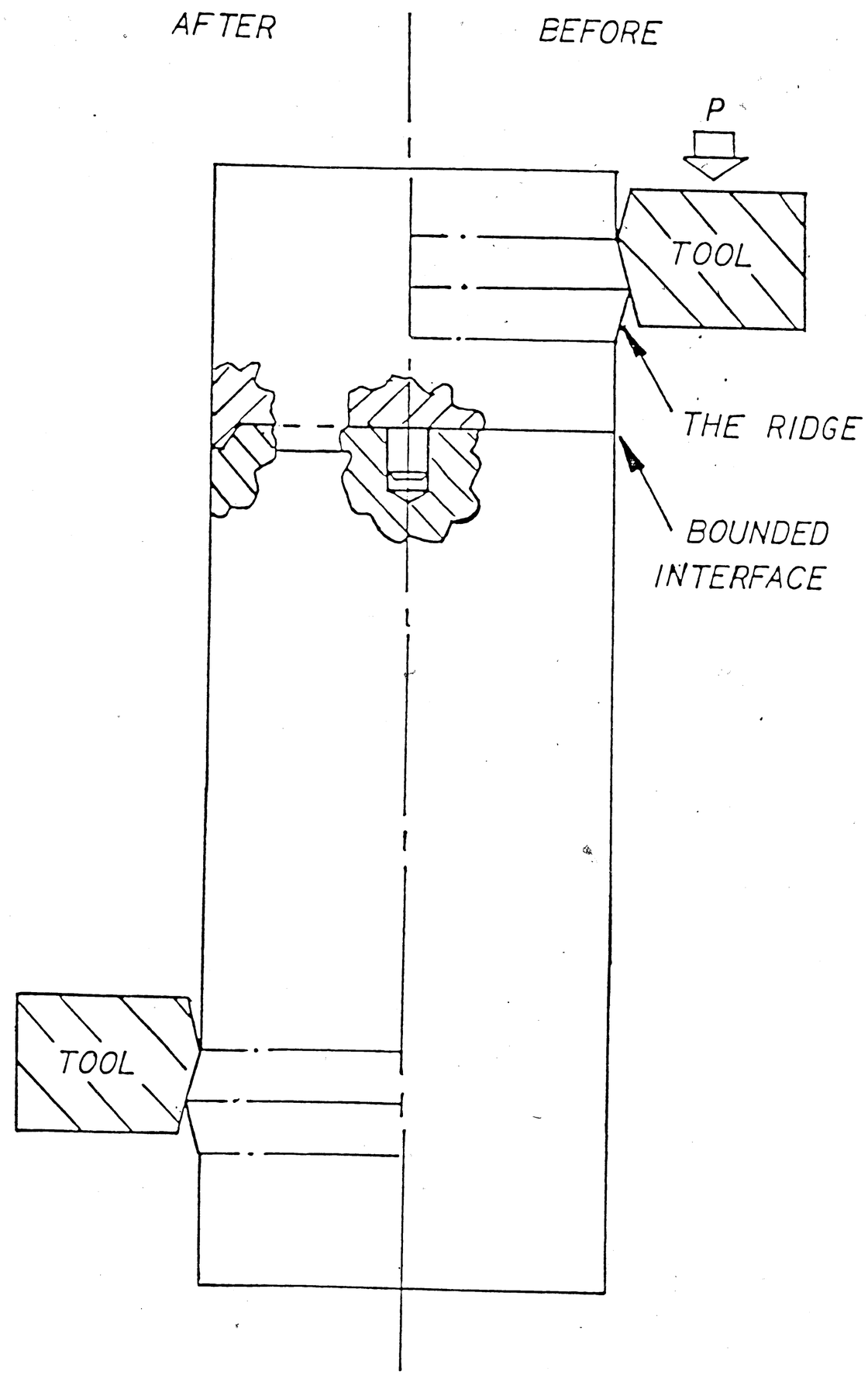

FIG. 1 THE MOBILITY OF THE RIDGE

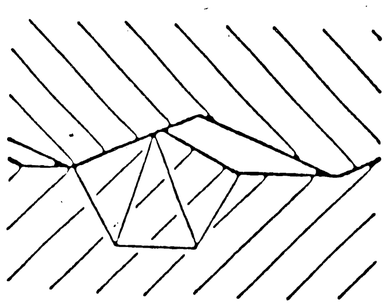

(a) *MOBILE*

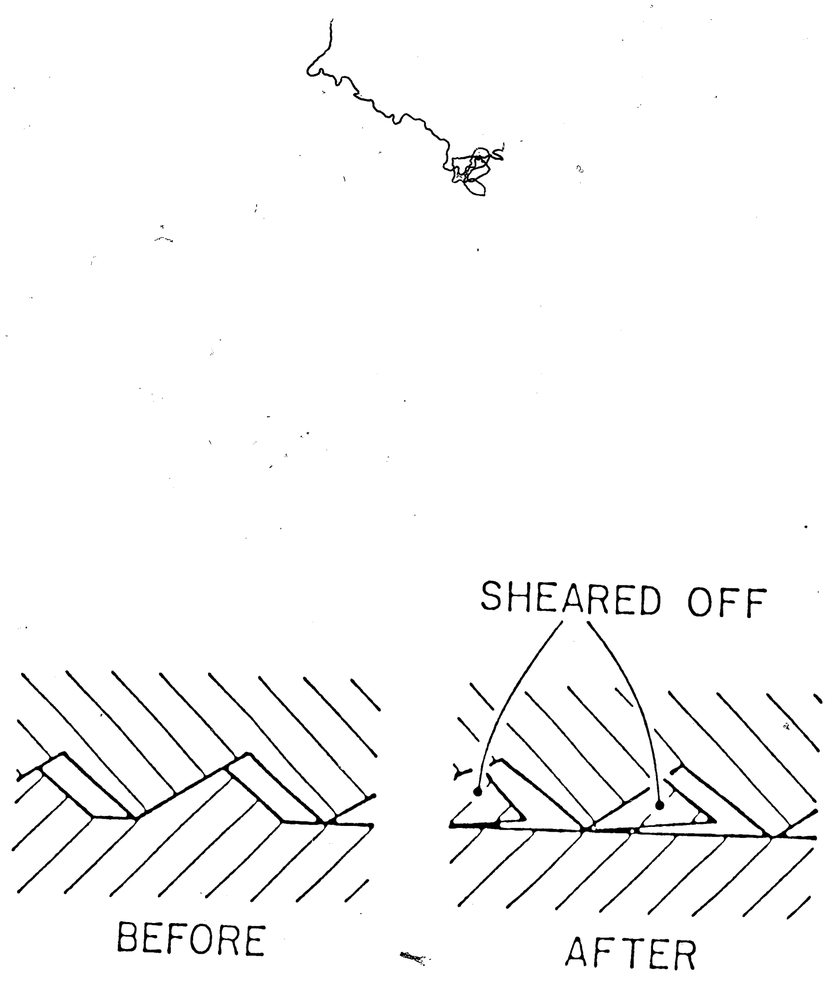

(b) *SHEARING*

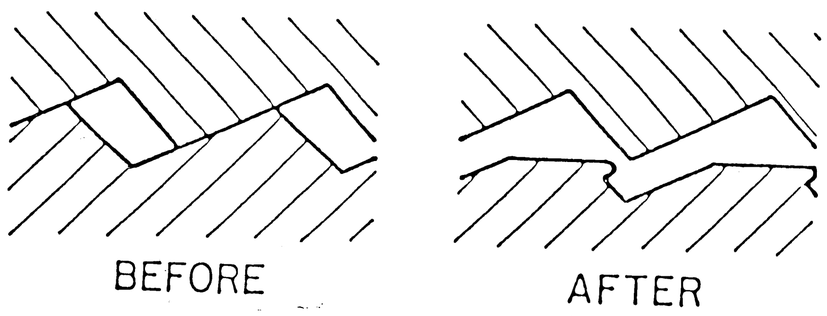

(c) *PLOWING*

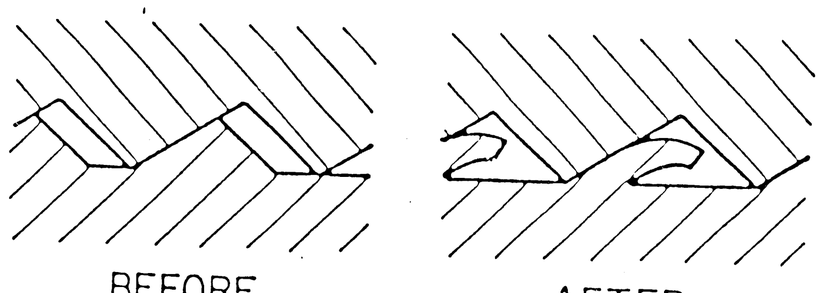

(d) *SHAVING*

FIG. 2 SEVERAL POSSIBLE PATTERNS FOR DISTORTION OF ASPERITIES

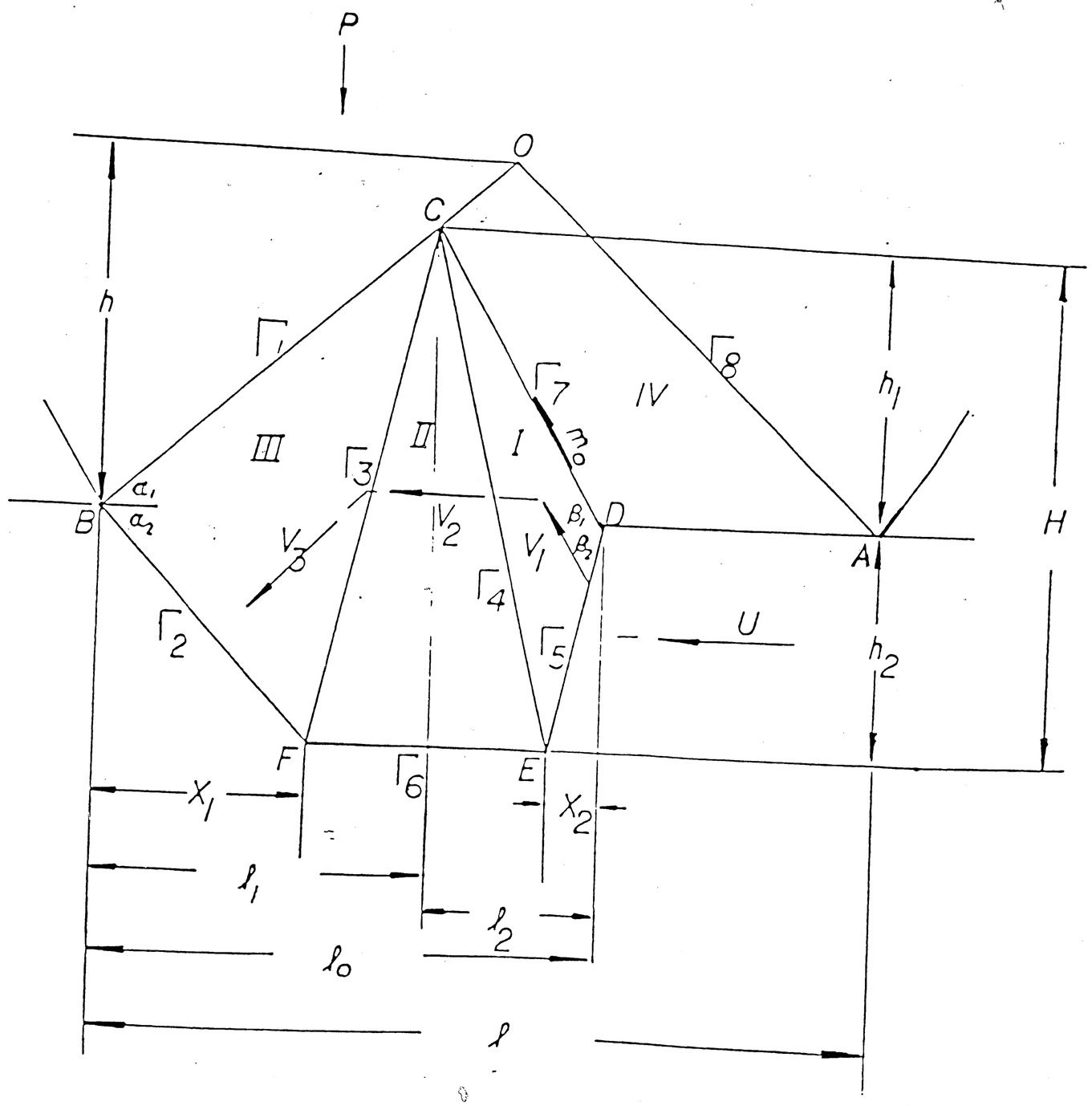

FIG. 3 TRI-TRIANGULAR VELOCITY FIELD

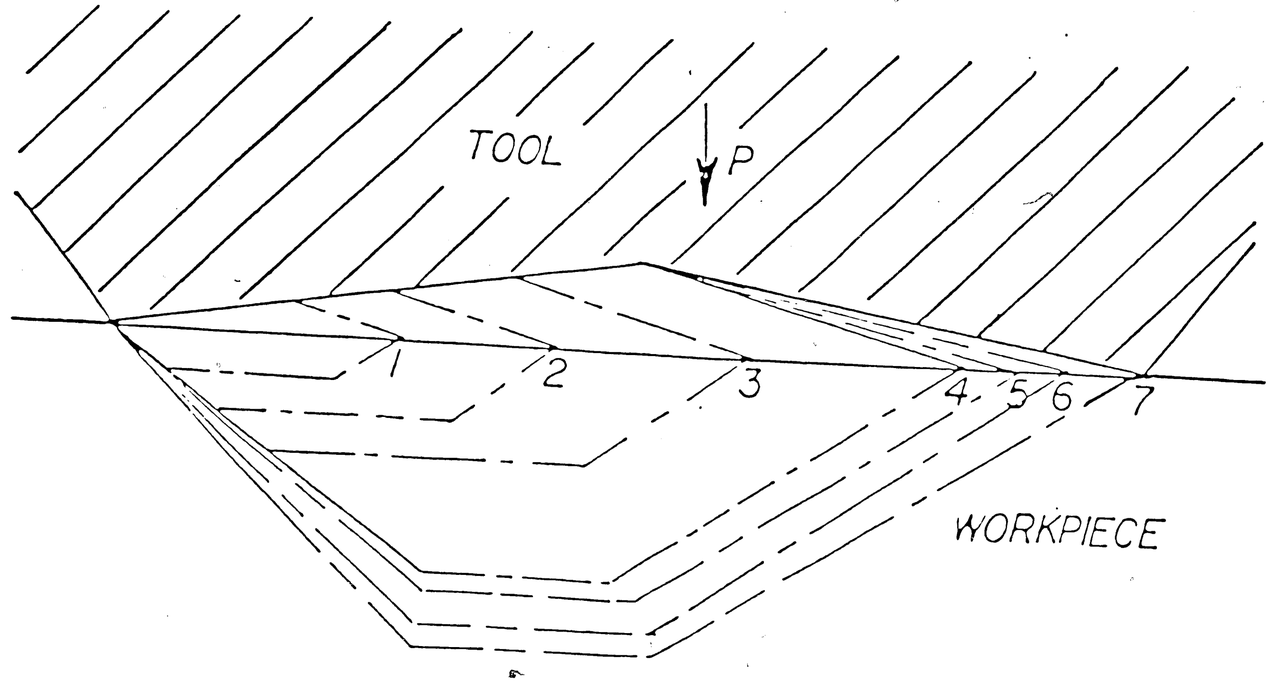

FIG. 4 SCHEMATIC DESCRIPTION OF THE GROWTH OF THE RIDGE WITH INCREASING FORCE

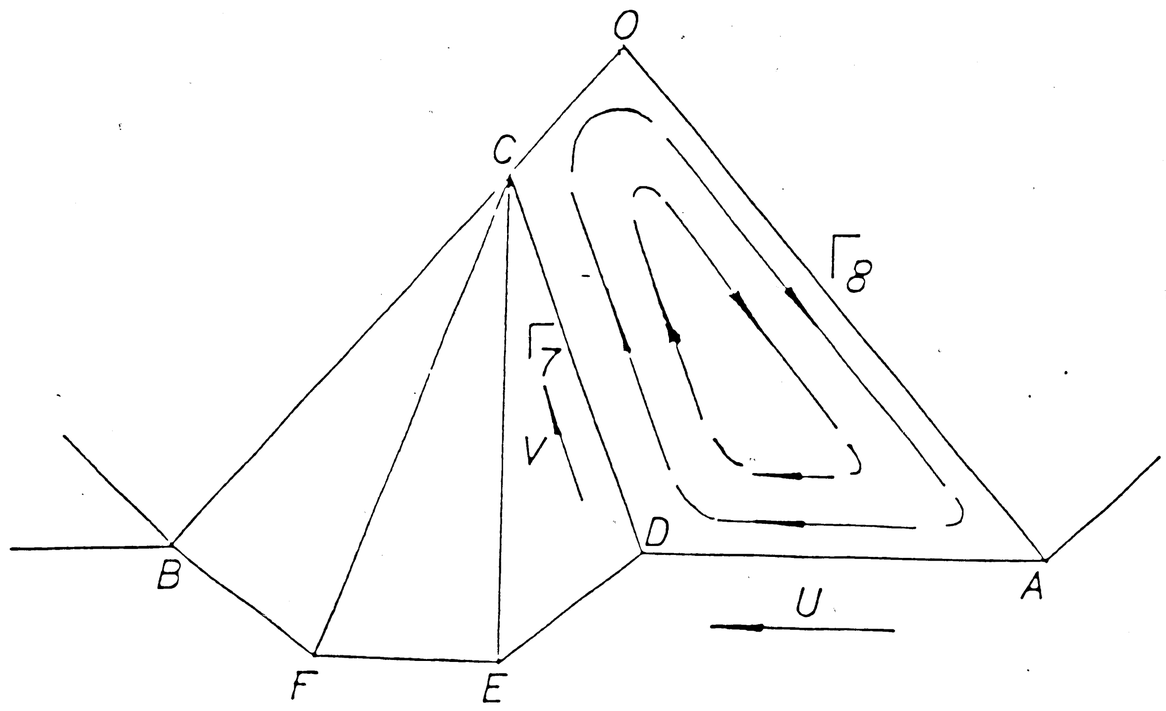

FIG.5 SCHEMATIC SHOW OF FLOW PATTERN IN LIQUID POOL

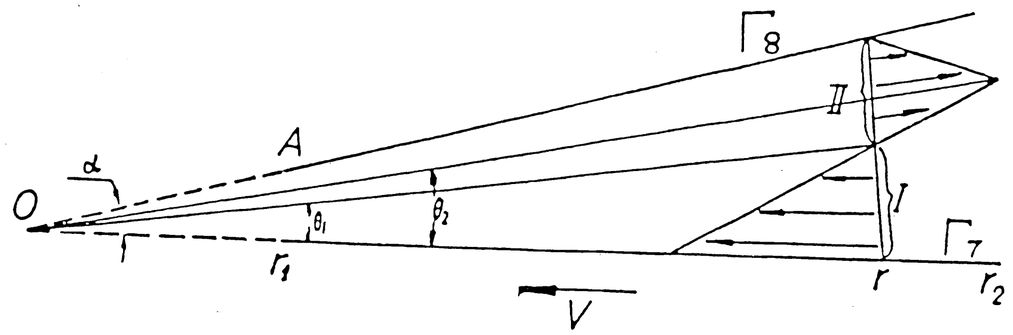

<a>

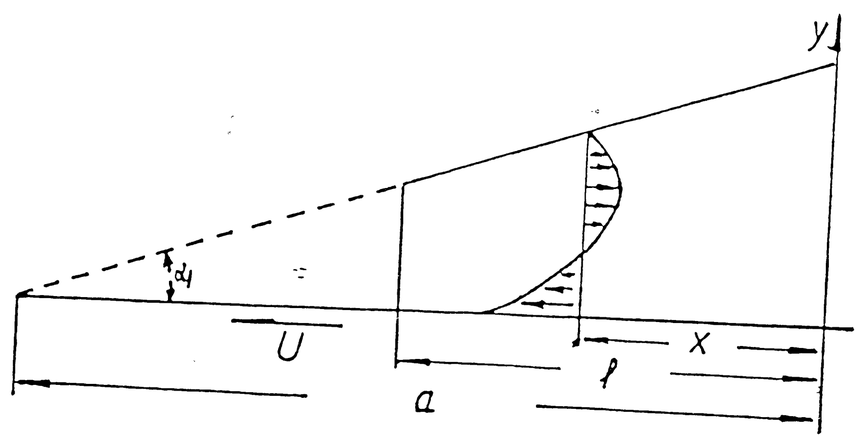

<b>

FIG.6 VELOCITY FIELD OF <a> BOUNDARY LUBRICATION; <b> HYDRODYNAMIC LUBRICATION I AND II DESIGNATE TWO FLOW CROSS SECTION

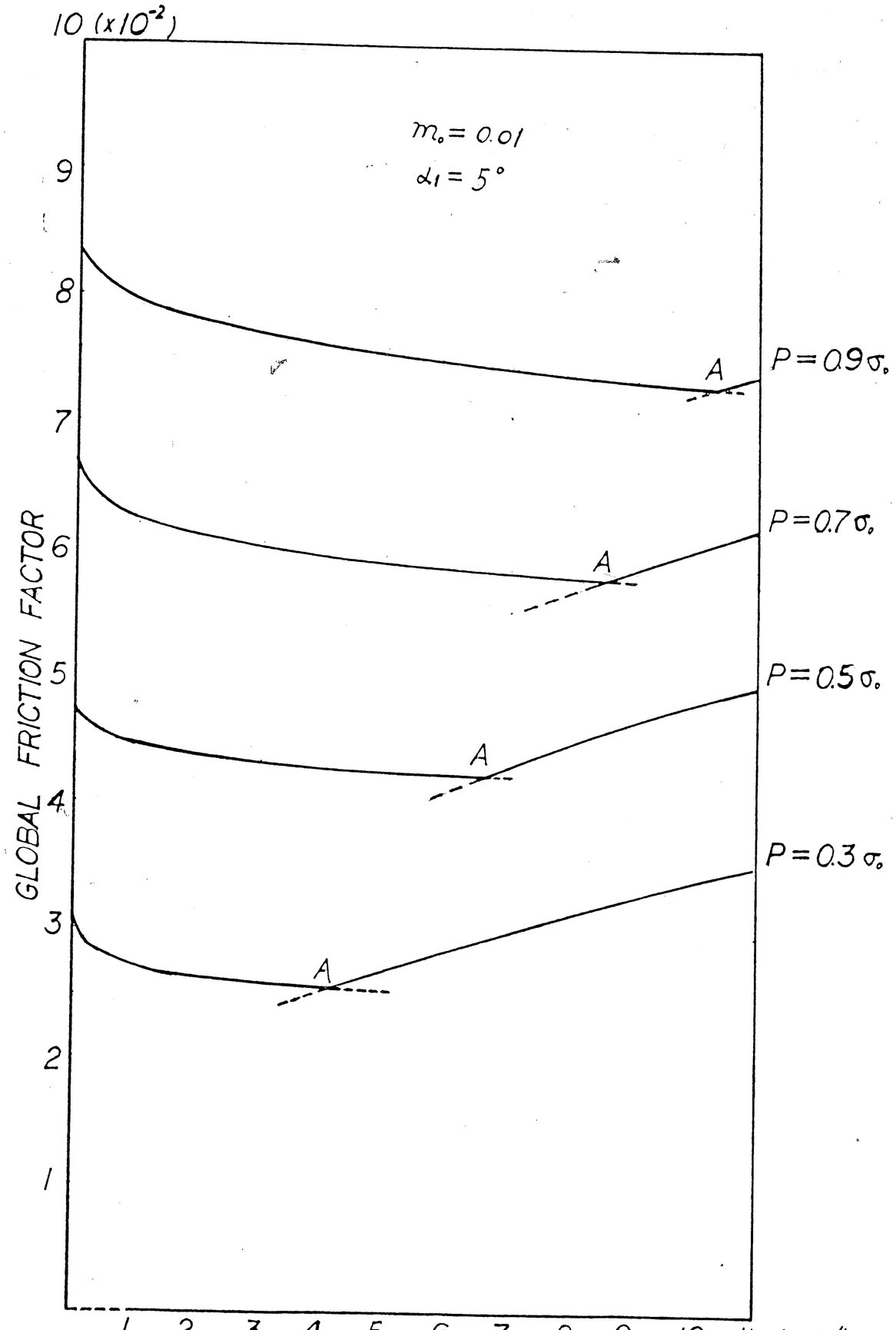

FIG.7a GLOBAL FRICTION FACTOR VS. SOMMERFELD NUMBER MIXED LUBRICATION, ON THE LEFT OF POINT A; HYDRODYNAMIC LUBRICATION, ON THE RIGHT OF POINT A.

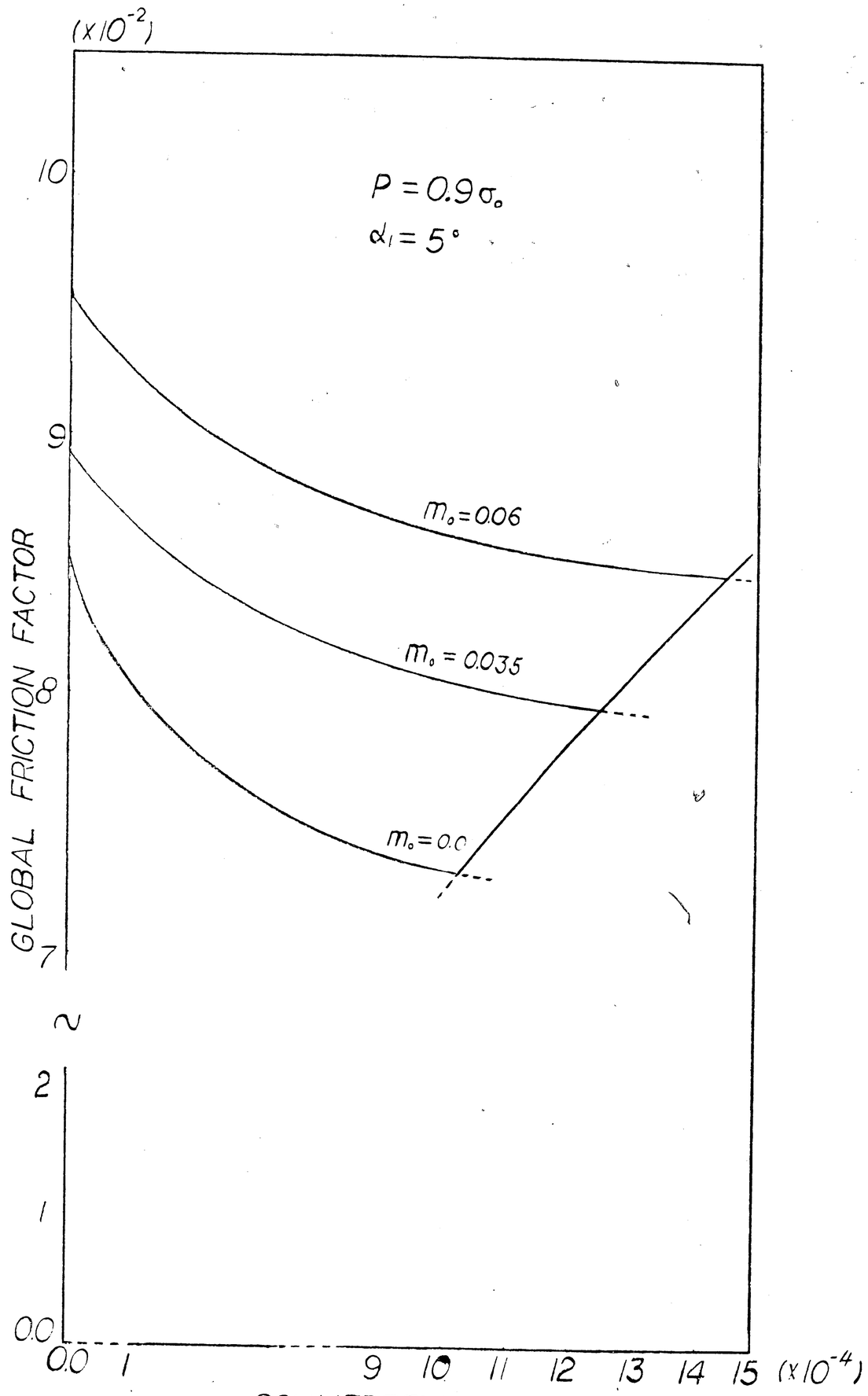

FIG. 7b LOCAL FRICTION FACTOR m_0 AS PARAMETER

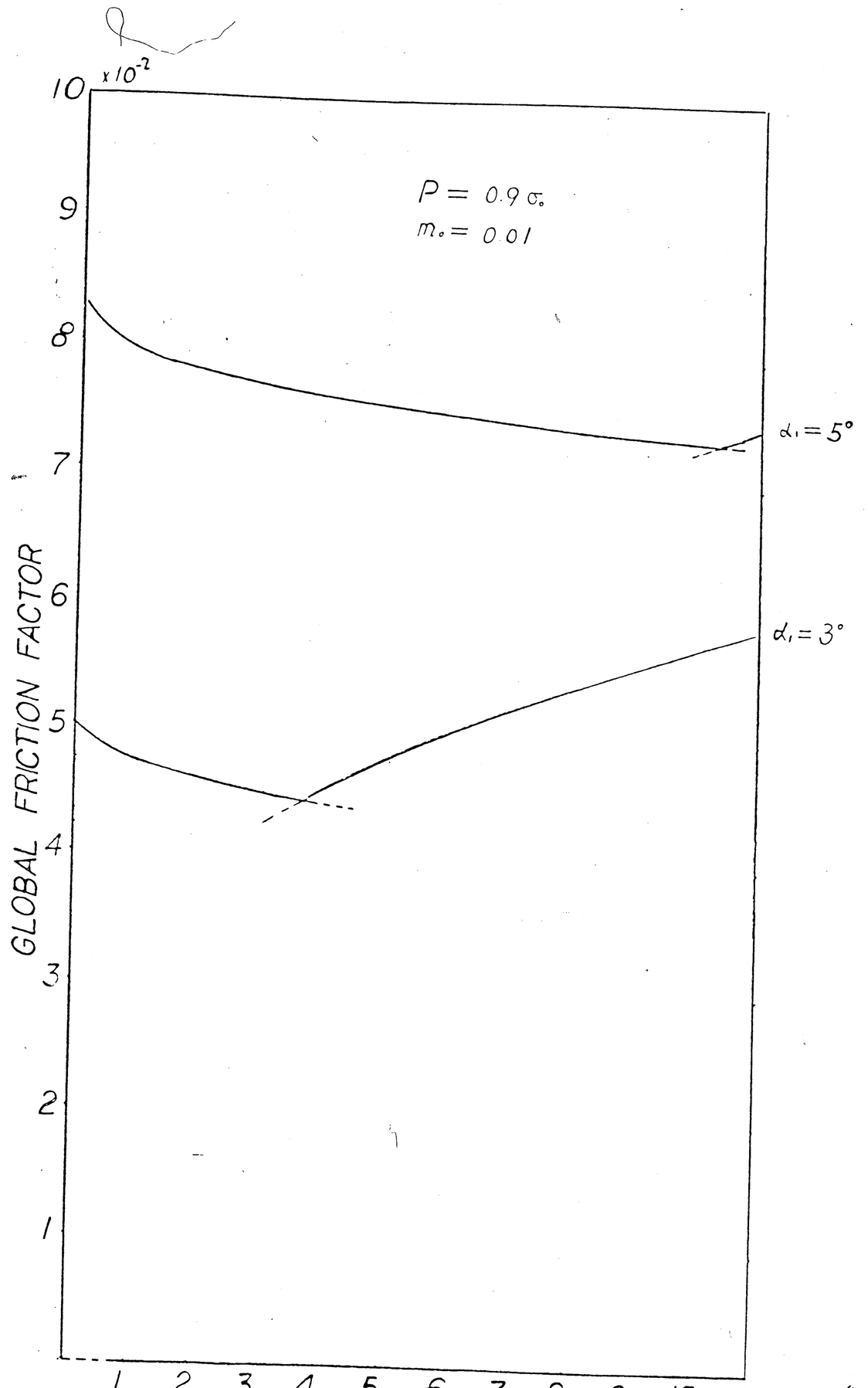

FIG. 7c WEDGE ANGLE α_1 AS PARAMETER

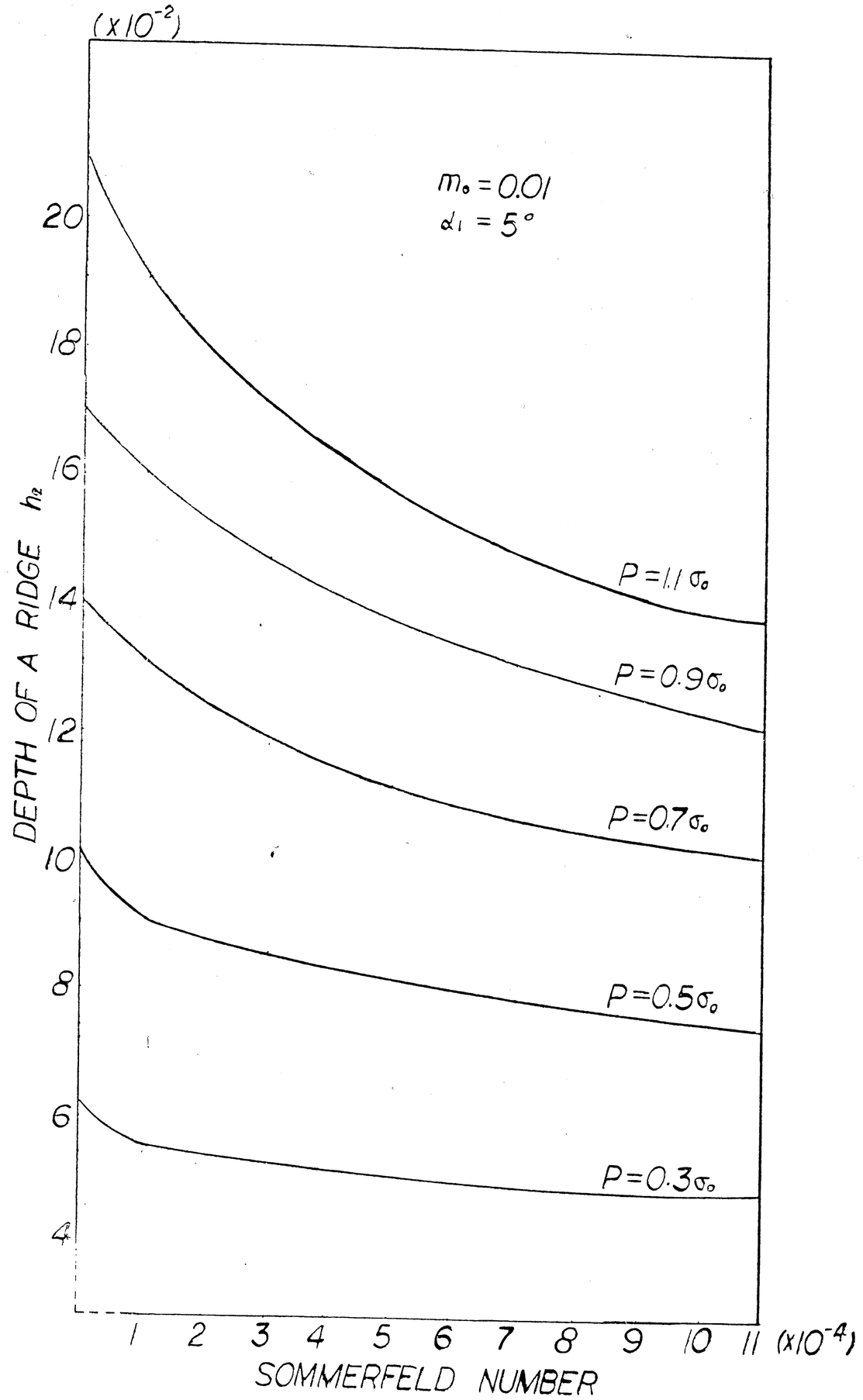

FIG. 8 h_2 vs. SOMMERFELD NUMBER

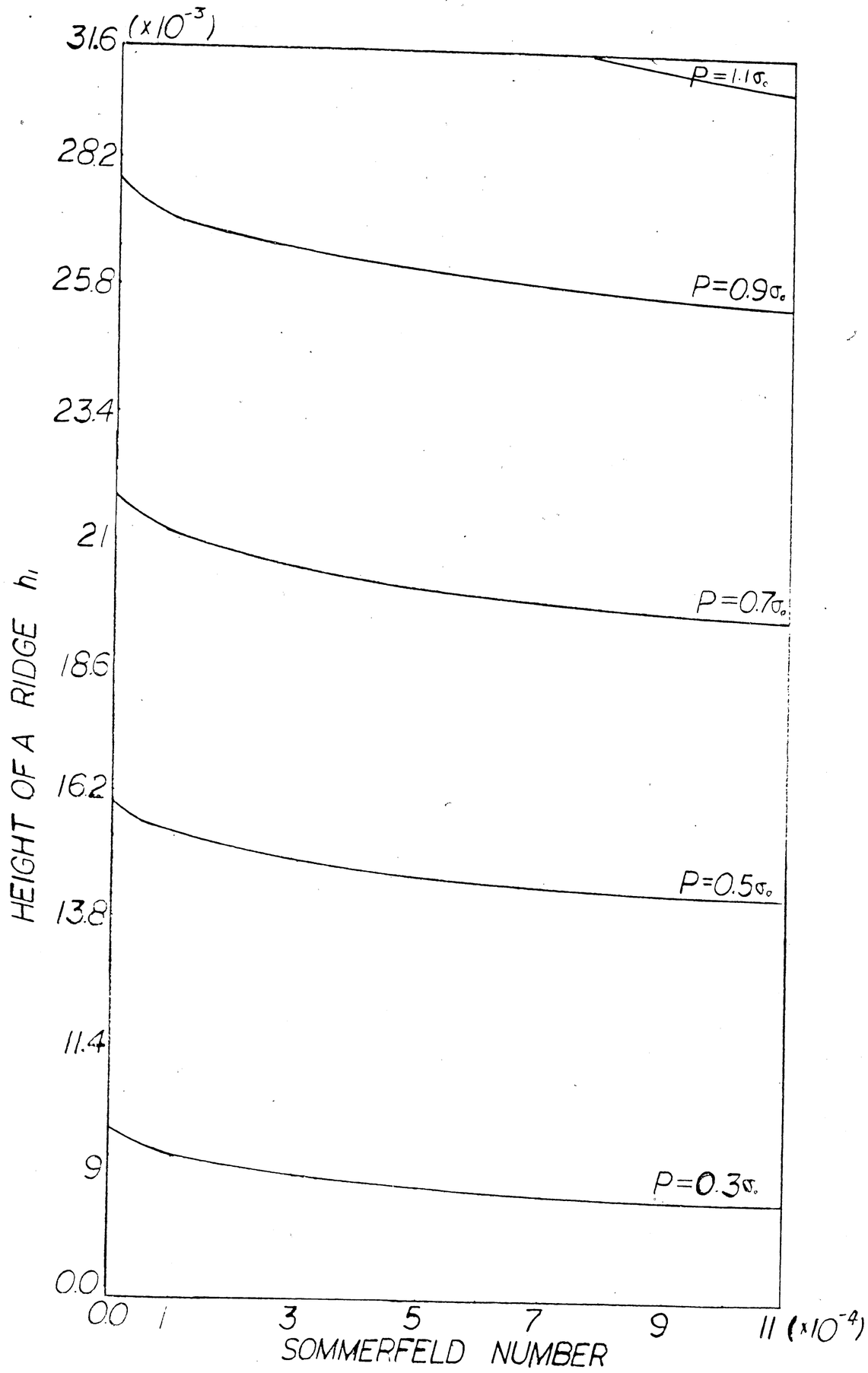

FIG. 9 h_1 vs. SOMMERFELD NUMBER

FIG.<10> FRICTION FACTOR vs. APPLIED FORCE

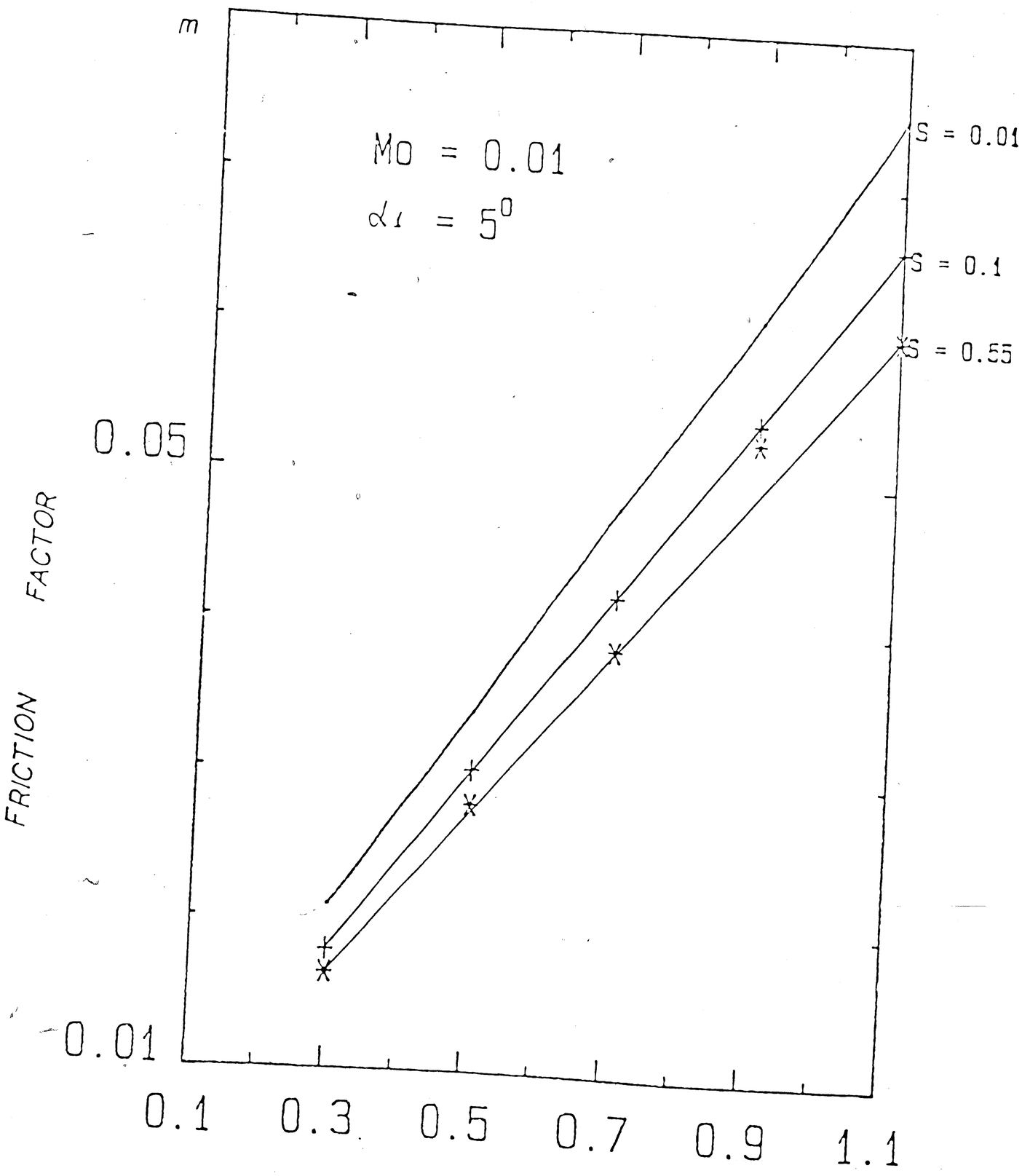

12 Vita

Name : Tao Liu

Date of Birth : July 1, 1963

Place of Birth : Beijing, People's Republic of China

Name of Father : Kuo-xun Liu

Name of Mother : Zhuo-ming Guan

Institutions attended : University of Peking, Beijing, P.R.O.C.

Degree : Bachelor of Science, July, 1985

An Upper-Bound Approach to Liquid lubricated Friction in Steady State Sliding

by

Tao Liu

Abstract

Presented in this paper is a study of the mathematical modeling of the steady state sliding of two metal surfaces, based on the upper bound approach, and including both the simulation of friction and of lubrication effects. The existence of wedge-shaped protrusions on the tool surface is assumed. Pressing these protrusions into the workpiece and sliding the tool along the workpiece produces asperities on its surface. Therefore, the formation of these asperities is caused by the plastic deformation through a specified depth under the surface. Growth of these asperities is arrested by the high pressure developed in the thin layer of lubricant trapped in the gaps between the asperities of the interfacing surfaces. The combination of the energy dissipated in the deformation of a thin layer under the surface, local resistant force to sliding along the interface, and the energy consumed in the lubricant produces a global resistance to sliding. The global resistance to sliding is a function of a Sommerfeld number, which is a dimensionless parameter : $S=\frac{\eta \cdot U}{\sigma_0 \cdot l}$, where η is the viscosity, U is the working speed, σ_0 is the flow strength of the workpiece, and l is average length of wedges. Global resistance to sliding decreases with increasing values of S until the global resistance reaches a minimum value; it then increases with further increase in S. The minimum value of global resistance is reached when full seperation by a thin lubricant film is established between the two solids. This phenomenon is called " hydrodynamic lubrication ". The resistance to sliding is

related to the geometry of the asperities at the surface of the tool, to the Sommerfeld number ,S, and also to the constant friction factor, which is used for measuring a local frictional force where metal-to-metal contact prevails along the interfaces of the opposing asperities.

An Upper-Bound Approach to Liquid lubricated Friction in Steady State Sliding

by

Tao Liu

Abstract

Presented in this paper is a study of the mathematical modeling of the steady state sliding of two metal surfaces, based on the upper bound approach, and including both the simulation of friction and of lubrication effects. The existence of wedge-shaped protrusions on the tool surface is assumed. Pressing these protrusions into the workpiece and sliding the tool along the workpiece produces asperities on its surface. Therefore, the formation of these asperities is caused by the plastic deformation through a specified depth under the surface. Growth of these asperities is arrested by the high pressure developed in the thin layer of lubricant trapped in the gaps between the asperities of the interfacing surfaces. The combination of the energy dissipated in the deformation of a thin layer under the surface, local resistant force to sliding along the interface, and the energy consumed in the lubricant produces a global resistance to sliding. The global resistance to sliding is a function of a Sommerfeld number, which is a dimensionless parameter : $S=\frac{\eta \cdot U}{\sigma_0 \cdot l}$, where η is the viscosity, U is the working speed, σ_0 is the flow strength of the workpiece, and l is average length of wedges. Global resistance to sliding decreases with increasing values of S until the global resistance reaches a minimum value; it then increases with further increase in S. The minimum value of global resistance is reached when full seperation by a thin lubricant film is established between the two solids. This phenomenon is called " hydrodynamic lubrication ". The resistance to sliding is

related to the geometry of the asperities at the surface of the tool, to the Sommerfeld number ,S, and also to the constant friction factor, which is used for measuring a local frictional force where metal-to-metal contact prevails along the interfaces of the opposing asperities.